

A multimaterial electrohydrodynamic jet (E-jet) printing system

This article has been downloaded from IOPscience. Please scroll down to see the full text article.

2012 J. Micromech. Microeng. 22 045008

(<http://iopscience.iop.org/0960-1317/22/4/045008>)

View [the table of contents for this issue](#), or go to the [journal homepage](#) for more

Download details:

IP Address: 130.126.101.238

The article was downloaded on 07/05/2012 at 22:45

Please note that [terms and conditions apply](#).

A multimaterial electrohydrodynamic jet (E-jet) printing system

E Sutanto, K Shigeta, Y K Kim, P G Graf, D J Hoelzle, K L Barton,
A G Alleyne, P M Ferreira and J A Rogers

University of Illinois, Urbana, IL 61801, USA

E-mail: alleyne@illinois.edu

Received 17 September 2011, in final form 19 December 2011

Published 15 March 2012

Online at stacks.iop.org/JMM/22/045008

Abstract

Electrohydrodynamic jet (E-jet) printing has emerged as a high-resolution alternative to other forms of direct solution-based fabrication approaches, such as ink-jet printing. This paper discusses the design, integration and operation of a unique E-jet printing platform. The uniqueness lies in the ability to utilize multiple materials in the same overall print-head, thereby enabling increased degrees of heterogeneous integration of different functionalities on a single substrate. By utilizing multiple individual print-heads, with a carousel indexing among them, increased material flexibility is achieved. The hardware design and system operation for a relatively inexpensive system are developed and presented. Crossover interconnects and multiple fluorescent tagged proteins, demonstrating printed electronics and biological sensing applications, respectively.

(Some figures may appear in colour only in the online journal)

1. Introduction

Nano and micro-manufacturing has emerged as a critical component of nano and micro systems technology. Along with an increasing variety of available materials comes a need for increasingly sophisticated manufacturing platforms capable of utilizing said materials at higher and higher levels of resolution. As a consequence, research efforts to utilize graphic arts printing for demanding applications, such as printed electronics and biological sensors, have grown rapidly in the past few years. Inkjet printers utilize thermal or mechanical (piezo-driven) excitation to reliably print features with a peak resolution of 10–30 μm [1] depending on the specific technology. This resolution limit results from the combination of minimum droplet size ($\sim 10\text{--}20\ \mu\text{m}$) and placement errors ($\sim \pm 10\ \mu\text{m}$) at a 1 mm standoff distance [2, 3]. While suitable for a wide variety of applications, the use of conventional graphic arts approaches such as inkjet printing cannot be used for manufacturing higher resolution products with feature resolutions of 1 μm or better.

Electrohydrodynamic jet (E-jet) printing is an alternate printing technique for solution-based deposition applications requiring resolutions between 100 nm and 10 μm [4–6]. Recent advancements in E-jet printing speed and reliability

[4, 5] have transformed this technology from a research tool to a viable manufacturing process with droplet depositions possible at frequencies above several kHz. Additionally, design efforts made E-jet systems affordable, now in line with those of conventional ink-jet systems. Barton *et al* [6] recently developed a compact and affordable (<\$50 000 US) E-jet printing system, thereby making the process more accessible to researchers both in industry and academia. In addition to the ability to print high-resolution features, in [7] E-jet's ability to print using a large variety of functional inks including metallic inks (e.g. Ag), polymers and biological materials was demonstrated.

While promising and demonstrating feasibility of the high-speed/high-resolution E-jet concepts, most previous E-jet activities have focused on the printing capabilities of a single nozzle with a single material solution. Heterogeneously integrated functional electronic systems often require multiple materials (polymers, metals, biological material) to be present and collocated on the same substrate. It is this demand for more complex, multimaterial functionality that leads to the need for an E-jet printing tool capable of depositing multiple material inks with the same speed and resolution as previously demonstrated systems. The results in this paper present a new design for E-jet printing systems akin to early pen plotters of

the computer industry [8]. The design objective is to replicate the successful printing capabilities of single material single unit E-jet printing in a multiple syringes configuration. Each element of the carousel can carry an independent material ink thereby creating a multimaterial multiunit system. Since the parameters associated with individual unit E-jet print nozzles have been previously developed the key remaining challenges are the appropriate mechanical system design and the operation of the multiunit system. In particular, the operational challenge involves the ability to accurately index selected print nozzles with a resolution sufficient for overlaying individual material droplets. This indexing and overlay registration must also be coupled with E-jet drop-on-demand (DOD) capabilities [4] to effect a practical system.

The rest of this paper is organized as follows. Section 2 presents the basic principle of E-jet printing technology. Section 3 presents the challenge and solutions for mechanical design and fabrication of a multiunit E-Jet print-head. Section 3 also describes the integration of the new print-head into an existing [9] E-jet platform. Section 4 provides the solution for the operational challenges associated with indexing the print-head with respect to the desired substrate location to allow overlay and DOD with multiple materials. A two-stage macro-micro-positioning approach is used that incorporates vision-based feedback control for the micro-positioning. Section 5 provides two separate example applications demonstrating the advantages of the added functionality; one from printed electronics and one from biological sensing. A conclusion in section 6 provides an overview of the main contributions and highlights future directions for this promising technology.

2. Electrohydrodynamic-jet printing background

E-jet printing uses an electric field to induce fluid flows from micro capillary nozzles to create devices in the micro/nano-scale range [7]. The E-jet printer as well as the printing process is detailed in [10] and various coloured ink droplets were dispensed into uniform patterns on a thick paper or transparency that is placed beneath a conductive plate. These methods easily surpassed the conventional state of the art ink-jet technology at the time. Nevertheless, further manufacturing issues such as speed/throughput, droplet resolution/repeatability, ink variations and potential applications of the process were not clearly addressed until [7] was published.

Figure 1 illustrates the basic components of an E-jet system; these include an ink chamber, conducting nozzle, substrate and translational stage. The inset shows the conductive nozzle for a sense of scale. In addition to the unit hardware, a computer and DAQ interface that varies the tuneable system parameters including applied voltage, back pressure and standoff distance between the nozzle tip and the substrate. These process parameters are dependent on the ink material, nozzle diameter and substrate material. For a constant voltage potential between nozzle and substrate, Choi *et al* proposed the relationship of the droplet frequency, f , applied voltage, V and the stand-off height, h , to be as follows:

$$f = K \left(\frac{V}{h} \right)^{3/2} . \quad (1)$$

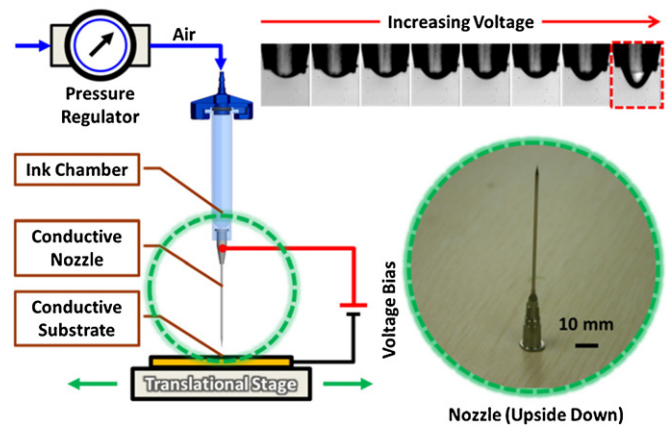


Figure 1. Schematic of a standard E-jet printer.

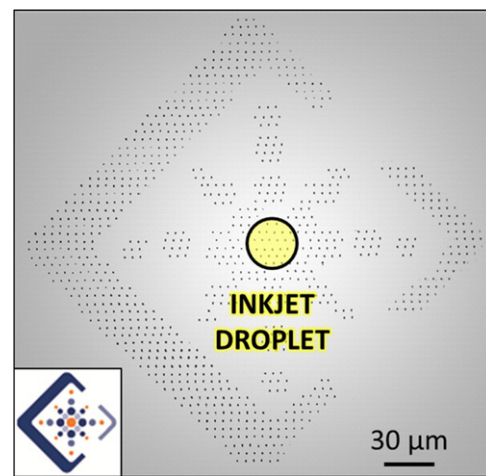


Figure 2. E-jet and inkjet droplet size comparison.

In (1), K is a scaling factor which is dependent on the process parameters [10].

To achieve printing, the back pressure in the ink chamber pushes the ink through the nozzle towards the tip. The applied voltage generates an electric field between the nozzle and the substrate causing concentration of charge on the pendant drop emanating from the tip. This concentrated charge generates shear stress, deforming the meniscus to a conical shape [7] termed a Taylor cone. The shear stress generated by the charge overcomes the ink surface tension; thereby releasing a droplet. As the applied voltage increases, the printing process will transition through various printing modes (e.g. pre-jet, continuous jetting, spraying). To control the precision of the drop emission process in [4] a pulsed mode E-jet system which modulates the applied voltage profile to achieve individual drop on demand printing was introduced. As one benchmark of resolution superiority, figure 2 illustrates the difference between an E-jet printing with 500 nm droplets and a high-quality ink-jet droplet with reference to the inset on the bottom left corner. The interested reader is referred to [4, 5, 7] for further results of E-jet flexibility, speed and resolution.

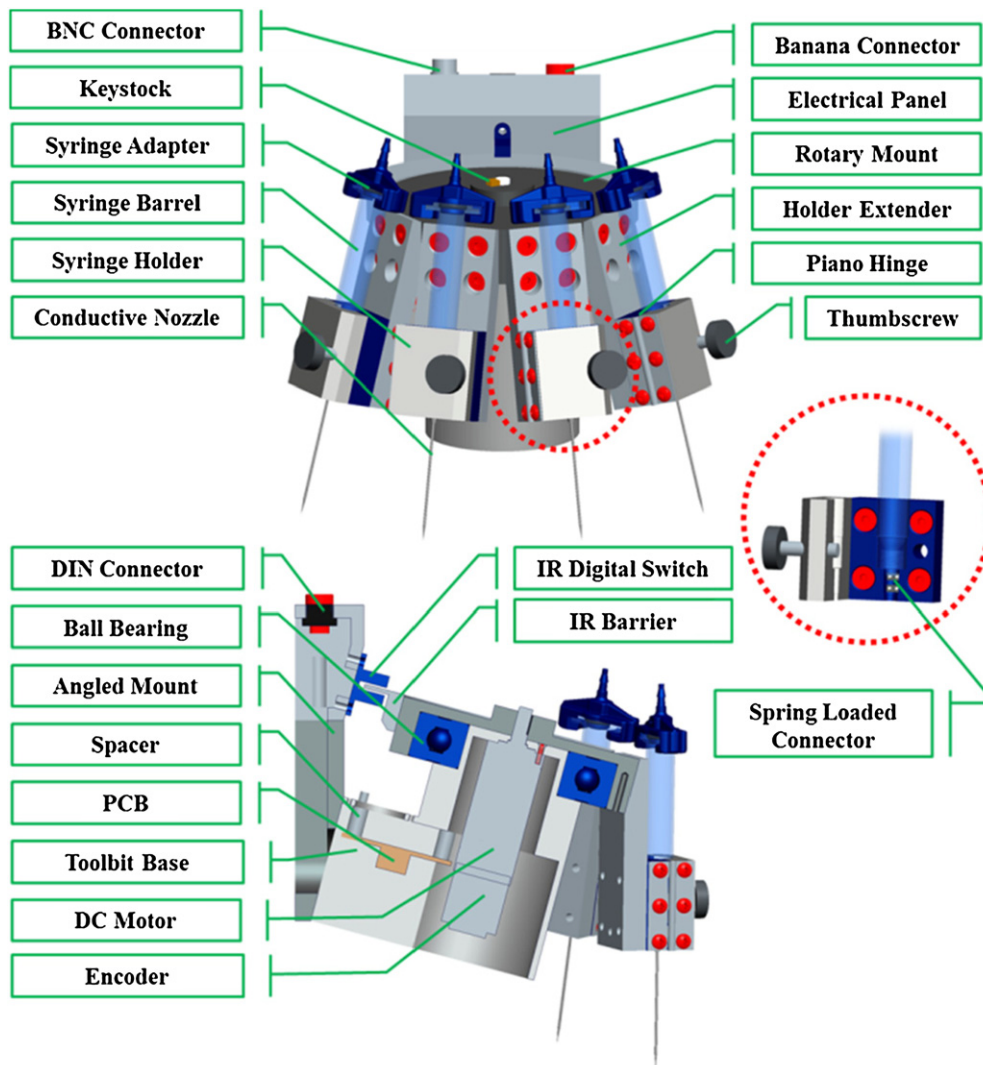


Figure 3. Mechanical components of the multiunit print-head.

3. Design of multiunit E-jet print-head

This section presents the details of the mechanical design for the multiunit E-jet print-head. In addition, we present the electronics and pneumatics layout to enable multiunit operation.

3.1. Mechanical design

E-jet printing requires a sufficiently high electric field to generate droplet emission; typically on the order of several hundred volts to a few kilovolts depending on processing conditions. Additionally, since field strength is closely related to the distance between terminals, it is important to closely maintain a desired stand-off height. In [7] a $30\ \mu\text{m}$ nominal printing distance for consistent printing at reasonable ($<1\ \text{kV}$) potentials was recommended. At this close proximity, any slight misalignment of the substrate causes significant stand-off distance variation between the nozzle and the substrate during substrate XY motion. This could cause inactive nozzles to impact the substrate and damage themselves or the part being fabricated. To avoid impingement, a tilted rotary design

is considered as illustrated in figure 3. By tilting the frame of rotation relative to the stand-off height z -axis, this design can regulate the height of the active printing nozzle while keeping the other inactive nozzles away from the substrate. The reader will note that the print-head shown in figure 3 can carry up to 4 units. This is not a limitation and small design modifications can easily expand this print-head approach to carry several more printing units if necessary. Details on the components of the print-head, along with CAD drawings of the subassemblies, can be found in [11]. A DC motor is used to actuate the entire carousel. The motor body is mounted to the chassis base and the motor shaft is coupled to the carousel with a slot and key configuration. For safety, limit switches are integrated to the design to limit the rotational range of the entire print-head. The circuit board used to distribute the E-jet voltage signal to each active printing unit is mounted inside the print-head base. The circuit board is configured with a common ground and one high-voltage connection for each of the unit print systems carried by the rotary mount. The connections are spring loaded such that when the individual syringes in figure 3 are clamped using the hinge-thumbscrew mechanism,

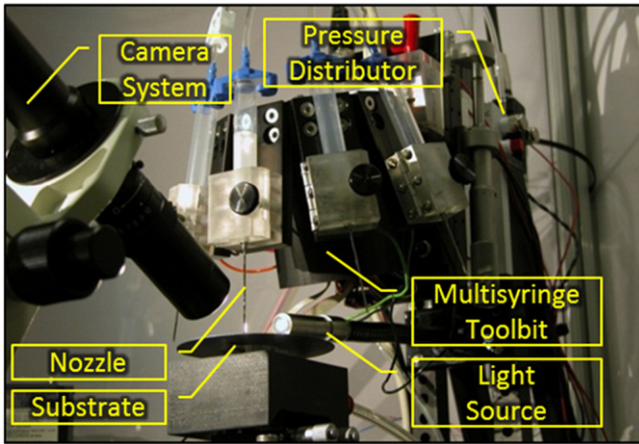


Figure 4. Integrated multiunit print-head system.

the nozzle tip will have potential difference with reference to the substrate.

To accommodate individual back pressure generation for each unit print system, a pressure distributor is integrated as an assembly of four pneumatic valves mounted on two pressure manifolds. This assembly is mounted on the motion stage which carries the entire print-head. By mounting the pressure generation subsystem off the print-head a great deal of space and weight can be saved thereby making the print-head more compact. Figure 4 shows the integration of the actual multiunit print-head.

3.2. Electronics system design

The electronics associated with the multiunit print-head are essential for its operation. These are used for sensing, actuation and control of the print-head. A data acquisition (DAQ) card (PCI-6229, National Instrument) is used to send and acquire signals to and from the on-board subsystems. Signals, such as the high-voltage E-jet pulsing signal and DC motor signal are amplified with individual signal amplifiers whereas other logic signals such as switches for pressure readings come directly

through the DAQ card signals. The DC motor is driven using a motor driver (25A8, AMC), powered by a power supply unit (PS300W24, AMC). As will be described in section 4, the indexing of the print-head requires two coordinated positioning approaches: macro- and micro-positioning. For macro-positioning, the motor uses an incremental magnetic encoder with a resolution of 512 counts per revolution for relative positioning.

The necessary voltage and pressure commands are distributed among the unit print-heads by switching the digital input/output (I/O) ports on the DAQ using solid-state optical relays (CLA187-ND, Digikey). A low power digital signal is sent to the relay which transmits this to a high-power signal that can be used to either drive a pressure valve in a manifold or a high-voltage printing signal. Figure 5 illustrates, for two-unit systems, the connections among the low-power digital I/O control signals, the relays and the pressure or voltage outputs to the individual units. To distribute the printing voltage, the high-voltage connection from the printing amplifier (677B-L-CE, Trek) is connected to the inlet (#6 and #8) and the conducting nozzles are connected to the output side (#5 and #7). This configuration can be replicated for print-heads carrying more than two units.

All tool-bit functionalities are integrated using LabVIEW (National Instruments) and details of the interface can be found in [11].

4. Operation of a multiunit E-jet print head

The operation of a multiunit E-jet print-head differs from a single-unit one primarily in the indexing of units for printing. Accurate positioning of the nozzle with respect to the substrate after successive unit changes is the major challenge in the print-head design. This section discusses a two-stage process for accurately overlaying one unit's end position with a subsequent one's starting position. This will involve design and operation of a switching servo control algorithm.

This section first presents a system representation suitable for macro-scale positioning, including the response from

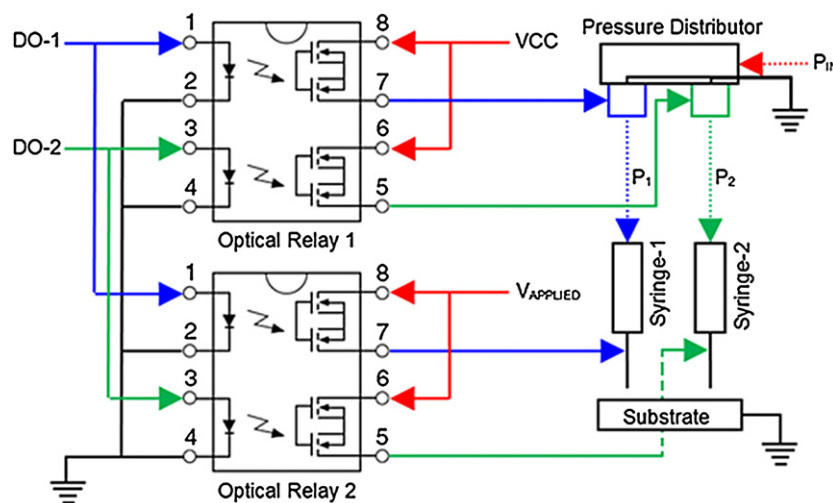


Figure 5. Voltage and pressure distribution schematic for two-unit systems.

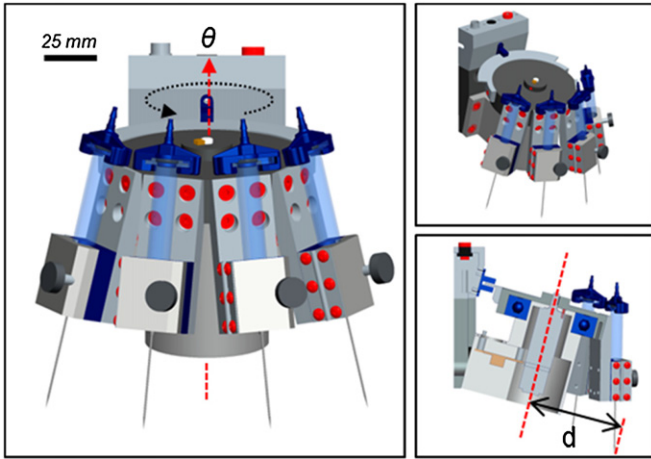


Figure 6. Multiunit print-head axis of rotation.

controller input to print-head rotation as measured by the on-board encoder. Next a vision-based measurement system is introduced. This vision-based system provides the micro-scale position information and also gives an inertial representation for the print unit nozzle tip with respect to the substrate position. This information is important for indexing one unit with respect to a previous one. A control architecture is then outlined briefly followed by a description and evaluation of designs for both stages of operation, micro- and macro-, during switching.

4.1. Print-head dynamic model

As described in section 3, the multiunit print-head is a carousel system driven by a DC motor as further illustrated in figure 6. Despite efforts to mount many of the mechanical and electrical systems off the print head, the mass of unit print-heads and their distance from the axis of rotation, coupled with the inherent mass of the carousel, provide a significant rotational inertia for the relatively compact drive system. In order to provide the necessary torque to rotate the head, the motor was supplemented by a mechanical transmission mechanism with a high gear ratio (1526:1). Despite its advantages, the transmission introduces operational control challenges. The backlash and stick-slip friction inevitably introduced by gearing deteriorate the ability to perform micro-positioning which is necessary for overlay registration and DOD operation.

To accomplish DOD operation, complete with overlay indexing, a high-performance positioning scheme is necessary. Based on a first principles analysis [12], the transfer function dynamics of the print-head can be represented in (2). Here, s is the Laplace Operator, $\theta(s)$ is the rotation of the print-head measured in degree and $U(s)$ is the control command in voltage sent from the DAQ system.

$$\frac{\Theta [s]}{U (s)} = \frac{K_P}{s (\tau_{PS} + 1)}. \quad (2)$$

Frequency domain system identification was performed to obtain the parameters of (2) with the system operating in a closed loop mode [12]. The obtained frequency response diagram is shown in figure 7. The resulting plant model using

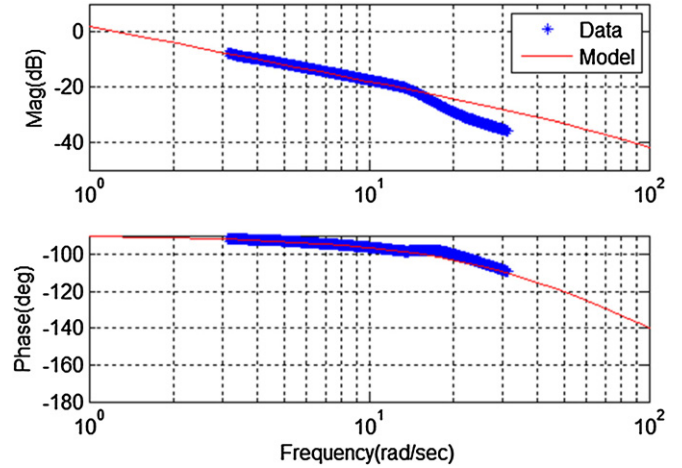


Figure 7. Bode plot of the multiunit print-head rotational dynamics.

the form of (2) is given in (3).

$$\frac{\Theta [s]}{U (s)} = \frac{1.25}{s \left(\frac{1}{85}s + 1 \right)}. \quad (3)$$

Equation (3) shows a system type of 1 [13]. This means that the print-head should theoretically have a zero steady-state regulation error for any constant position commands. As will be seen in section 4.4, this theoretical analysis overlooks additional physical phenomena, friction and backlash, that will need to be explicitly identified and compensated for.

4.2. Image processing and feature detection

The required encoder resolution, based on the tool-bit geometry shown in figure 6, is defined as

$$N = \frac{2\pi d}{\varepsilon}. \quad (4)$$

To position the nozzle tip within $2 \mu\text{m}$ accuracy ($\varepsilon = 2 \mu\text{m}$), it requires a resolution of approximately 60 000 counts per revolution. Encoders with this resolution are expensive and have a large physical envelope thereby making it difficult to integrate into a machine such as the one described in [6]. Moreover, the accurate positioning of the print-head mount with respect to its base does not guarantee that the print unit nozzles will be aligned with a desired location on the substrate. Here we to utilize a complementary sensing system that can provide higher resolution than an encoder and can simultaneously collocate the substrate and the nozzle tip. A vision system is the method of choice and the coarse resolution encoder is used to macro-position the active unit nozzle into the field of view of the camera for the micro-positioning system to take over.

Typically, E-jet printing requires the aid of a camera to monitor the printing process [6, 7, 9]; hence, no additional cost or complexity is incurred for implementing a vision based control scheme. The camera remains fixed with respect to inertial space; therefore, the micro-positioning is performed in an inertial reference frame. The vision system discussed in this paper operates at a sampling frequency of 10 Hz, sufficient to perform real-time position regulation.

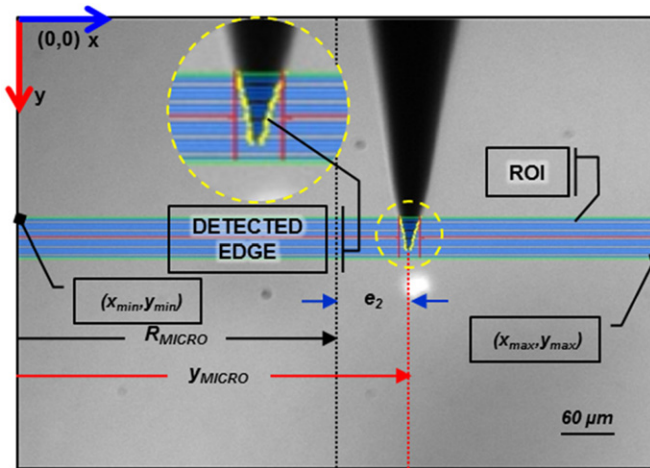


Figure 8. Edge detection for nozzle tip.

Applications that require high-speed transitions between individual printing units may need investments in higher speed cameras and processing hardware/software. The micro-positioning algorithm consists of four subroutines including (i) image capture, (ii) region of interest setting, (iii) feature detection and (iv) image analysis. Details on the algorithm presented here can be found in [11].

4.2.1. *Image capture.* Image capture is a critical step in the machine vision algorithm. Several parameters such as image resolution, camera frame rate, brightness and contrast are specified in this phase to ensure streams of high-quality pictures. Figure 8 illustrates a high-quality picture, where there is a good contrast between the background and the nozzle.

4.2.2. *Region of interest setting.* Setting a region of interest (ROI) is necessary to localize the nozzle position, hence reducing computation time. The ROI is also helpful in eliminating false edges. The ROI serves as the lower and upper bound of the image for which the feature detection will be performed. In this work, the ROI spans $[x_{min}, x_{max}]$ in the image's x -direction to keep track of the nozzle's lateral position. The nozzle tip is typically located slightly beneath the centre of the image in the image's y -direction. Therefore, the ROI must be identified, and possibly adjusted, according to the nozzle position in the image's y -direction. The ROI in figure 8 is indicated by the green box.

4.2.3. *Feature detection.* Here, an edge detection algorithm [14] is used to recognize the nozzle feature. Once the ROI is described, the feature detection subroutine will take place. A sample image is imported and the parameters associated with the edge detection are heuristically tuned such that the number of detected edges inside the ROI is maximized. Currently, these parameters have been optimized for the working conditions of the E-jet systems described in [11] and may have to be tuned in-place for other operational conditions. The yellow points, shown in figure 8, at the edge of the nozzle indicate the detected edges.

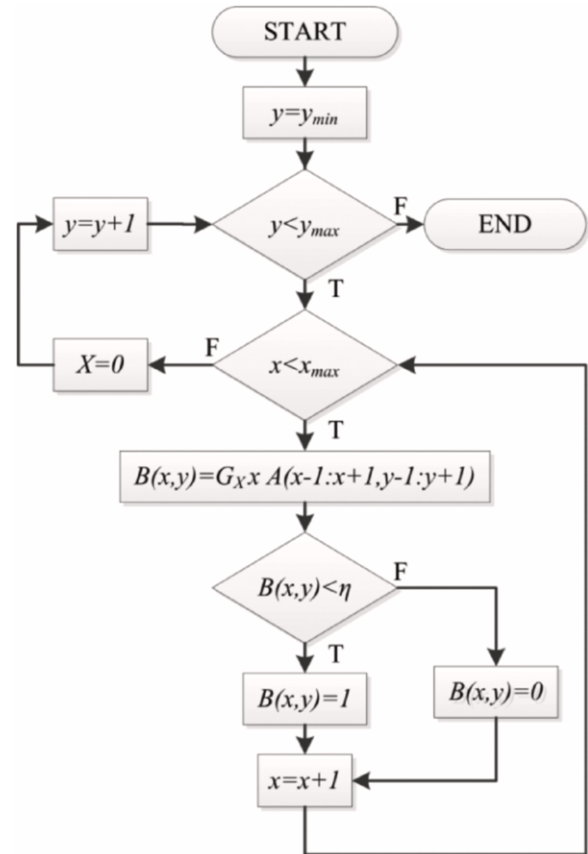


Figure 9. Edge detection algorithm.

In general, the nozzle edges can be detected by implementing the algorithm shown in figure 9. A 3 by 3 horizontal Sobel Operator Kernel [15] defined in (equation 5) filters every image pixel inside the ROI. The pixels inside the ROI, $A(x, y)$, are replaced by the transformed values in $B(x, y)$, which is a matrix multiplication of the Sobel Kernel, G_x , with the neighbouring pixels, $A(x - 1 : x + 1, y - 1 : y + 1)$ as shown in equation (6). The nozzle and the background image have a good opacity contrast as shown in figure 8. Hence, the Sobel Kernel will set a high value to the filtered image, $B(x, y)$. A pixel is recognized as an edge when $B(x, y)$ is larger than a threshold value, η . The filtering process is performed from the top left hand corner of the ROI in figure 8 to the bottom right hand corner of the ROI. Figure 13 illustrates the overall structure of the Edge Detection algorithm:

$$G_x = \begin{bmatrix} -1 & 0 & +1 \\ -2 & 0 & +2 \\ -1 & 0 & +1 \end{bmatrix} \quad (5)$$

$$B(x, y) = G_x * A(x - 1 : x + 1, y - 1 : y + 1). \quad (6)$$

4.2.4. *Analysis.* The detected edges carry position information with them and these values can be used to determine the position of the nozzle with respect to the camera. Since the camera is fixed, this position can also be used to infer the position of the nozzle tip with respect to the substrate. Assuming an axisymmetric nozzle, the lateral position of the tip, δ_x , can be described by (7), where n is the number of

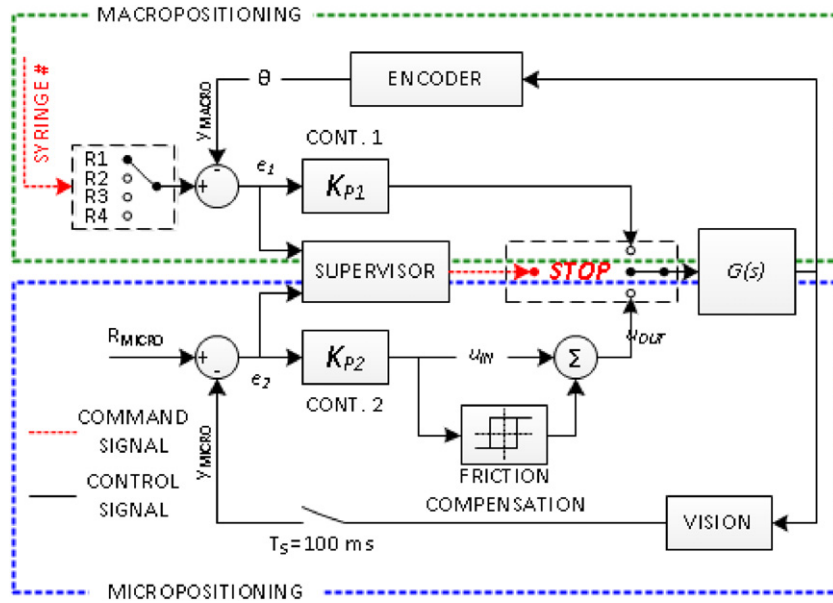


Figure 10. Dual macro- and micro-positioning system control architecture.

edges detected. The positional information is in terms of pixels and this must then be converted to displacement based on a calibration factor determined from the camera’s magnification.

$$\delta_x = \frac{\max(\delta_{x_i}) + \min(\delta_{x_i})}{2}; \quad i = 1 : n. \quad (7)$$

4.3. Control architecture

As indicated previously, the indexing between two print units has to be done in two steps: macro- and micro-positioning. The reference position for macro-positioning is defined in terms of the angle, θ , between the print-head based and the rotary mount as shown in figure 6. Alternately, the reference position for micro-positioning is defined in terms of pixels between the nozzle position and the pre-defined origin (0,0) coordinates within the ROI as seen in figure 8. The micro-positioning and macro-positioning have to work in unison for successful indexing and transition from one print unit to another. The overall positioning control architecture is illustrated in figure 10. The supervisor decides which controller to use based on the macro-positioning tracking error. For simplicity, both positioning schemes use a proportional-gain controller. Given the system type from equation (3), this is sufficient assuming the model is accurate.

The macro-positioning algorithm brings the nozzle into the camera field of view whereas the micro-positioning controller applies precise servo-level control to the nozzle position with respect to the substrate. The switch-over task done by the supervisor follows the algorithm described in figure 11. The tuning parameters α_1 and α_2 control the thresholds for handing over control between the macro- and micro-positioning control loops. Additionally, a tuneable dwell time constraint is added [16]. This is essential to avoid chattering back and forth between the two algorithms at the point of switch-over. For the purpose of this work, the dwell

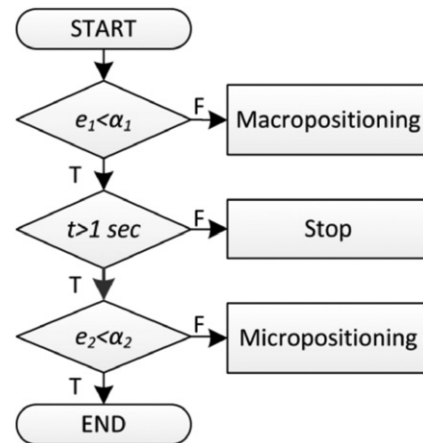


Figure 11. Supervisor switching logic.

time constraint was set at 1 second, but can be tuned if necessary.

It should be noted that other techniques exist and have been developed for the express purpose of switching between controllers. These include the family of so-called Anti-Windup/Bumpless Transfer controllers [17]. In the current case, the system comes to rest between controller implementations. Therefore, the necessity for any type of dynamic bumpless transition is eliminated. Should faster switching or transitions be a requirement in the future, it would be necessary to revisit the design of the switching mechanism from the very rudimentary, albeit sufficiently effective, effort used here.

4.4. Feedback control design

For simplicity, the authors assume that the vision system dynamics are sufficiently fast to perform a digital control design based on a discretization of the plant in equation (8). Based on the Internal Model

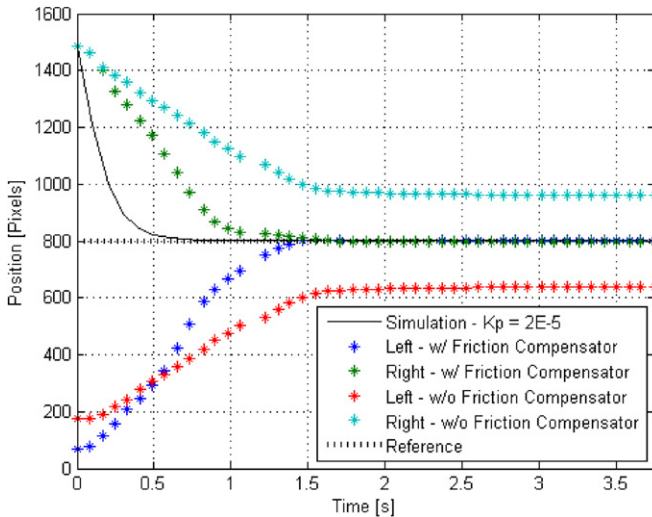


Figure 12. Friction effects on print-head rotation servo control.

Principle [13], proportional control should be sufficient to produce zero steady state regulation error for a constant commanded position. At a sampling frequency of 10 Hz, the zero-order hold [18] discrete time model of the closed loop system, G_{CL} , is shown in (8). Stability analysis in [19] indicates that the maximum value of the proportional gain, K_P , should be less than $2E-5$ V/pixel.

$$G_{CL}(z) = \frac{K_P(488.2z + 455.1)}{z^2 + (488.2K_P - 1.81)z + 455.1K_P + 0.8098} \quad (8)$$

Figure 12 shows indexing of a print unit nozzle approaching the centre of the camera’s field of view for a proportional gain value of 1×10^{-4} V/pixel. The figure provides step responses from both the left and right sides of the image. As shown in figure 12, the actual response of the closed loop motor control is more damped than the model would suggest. Moreover, the steady state response does not go to zero as predicted and is approximately 200 pixels or, equivalently, $100 \mu\text{m}$. The reason behind this is the relatively large amount of friction in the system bearings and motor gearing transmission. As the nozzle approaches the reference, from either side, the error signal approaches zero as does the control input. When the control input is too low to overcome frictional forces, the print-head rotation stops; hence zero steady state error is not achieved.

A simple friction compensator shown in (9) helps in alleviating this problem. This approach provides additional control input to overcome the frictional forces that are always acting against the direction of motion. The friction compensator constant C^+ and C^- can be found by incrementing its value from zero until nozzle motion is detected by the vision system. The value of C may vary from one print unit to the others and also dependent on the direction of approach. However, a simple manual identification procedure is currently sufficient to identify it. Should the friction continue to be an issue in future multimaterial E-jet systems, such as the one shown in figure 12, approaches for adaptively identifying the friction may be utilized for the

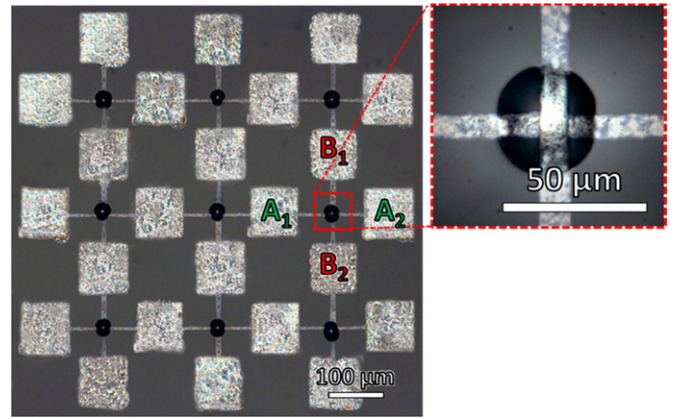


Figure 13. Crossover structure for Ag interconnect lines linking an array of Ag pads.

intended automation if the manual compensation proves to be to labour intensive.

$$u_{OUT} = \begin{cases} u_{IN} + |C_+|; & u_{IN} > 0 \\ u_{IN} - |C_-|; & u_{IN} < 0 \end{cases} \quad (9)$$

An additional benefit of the high-precision micro-positioning afforded by the vision feedback system is the ability to identify z -axis, or ‘stand-off height’, variations when indexing print-heads. It is possible for the nozzle tip of subsequent print-heads to be off by many microns. The vision feedback is able to measure this and compensate by vertically adjusting the substrate base. This can be performed manually or automatically if a motorized z -stage is available.

5. Multimaterial E-jet application

In order to explore the benefits and potential of the type of multimaterial E-jet printing system described in sections 2 and 3, we examine two separate application domains. In particular, we focus on printed electronics and biological sensors which have previously been examined as application areas for E-jet printing [7, 20]. For the case of printed electronics, we present the printing of multilayer interconnects that can be useful for versatile and flexible circuitry design. In the biological sensor domain, the results feature selective printing of multiple materials on a substrate by implementing DOD and provide sensor efficacy with small amounts of material.

5.1. Multilayer silver interconnects

Fuller *et al* among others, showed how multiple materials may be printed with ink-jet printing to fabricate complex functional electronic devices [21]. Similarly, complex functional electronic devices can also be fabricated using an E-jet printer and with much higher feature size resolution. Organic silver ink (TEC-IJ-010, Inktec) is used for printing a conductive silver line with one print unit and a photo-curable polymer (NOA-81, Norland Products) is printed by a second print unit in order to isolate the two intersecting conductive lines. In this work, fabrication of a crossover interconnect is demonstrated as shown in figure 13. The choice of the relatively thick line width for the silver interconnects ($\sim 12 \mu\text{m}$) is to maximize

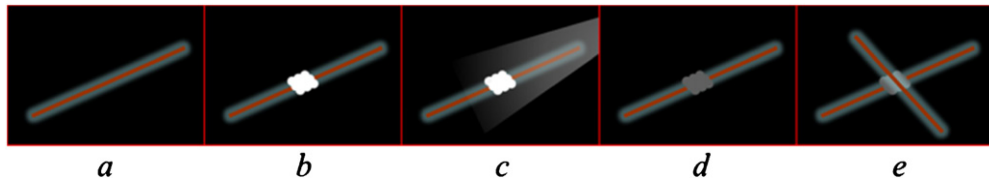


Figure 14. Step by step procedure to create a crossover interconnect structure.

Table 1. Silver interconnects conductivity measurement data.

Connection	Conductivity ($\Omega^{-1} \text{ cm}^{-1}$)
1 A ₁ – A ₂	7.864×10^4
2 B ₁ – B ₂	1.035×10^5
3 A ₁ – B ₁	–

conductivity of the connections. The results of the conductivity measurement, using a probe station, are presented in table 1, where A₁-A₂ and B₁-B₂ are the contact pads in figure 13 used to measure the conductivity of the lower and upper layer interconnects respectively. The connection between A₁-B₁ shows no connectivity thereby demonstrating the isolation.

The step by step procedures to fabricate the crossover structure are illustrated in figure 14. The silver ink is first printed on a silicon wafer substrate coated with Polyimide (a). NOA 81 is then printed on top of the silver at the crossover locations (b). Exposure of UV-light at 2 J/cm² and 365 nm wavelengths cures the polymer and create an insulation layer for the subsequent silver lines passing over the NOA insulators (c) and (d). Note that the curing time depends on the intensity of the UV source that is used. Finally, the second layer of silver interconnects are printed passing over the cured polymer (e).

The AFM image, and cross-sectional profile, in figure 15 give detailed information on the performance of each unit printing system. In particular, the profile shows the cured NOA adds a layer of approximately 3 μm on top of the original silver printed line, sufficiently thick to create an insulation layer. The E-jet printed silver interconnects demonstrated here are about 12 μm in width and 50 nm thick as shown in the AFM image in figure 15. This gives an overall validation of the ability to create printed interconnects and insulating overlays in the same platform. While the printing of individual silver lines at these resolutions, and below, can be easily accomplished with current E-jet processes, the ability to overlay NOA, or any other insulator, in a rapid and cost effective fashion is a unique feature of the multimaterial E-jet design.

5.2. Biological multimaterial application

Another application of current E-jet systems is the printing of biological materials [22]. Overlaying or creating patterns of multiple biological materials could be very useful for combinatorial studies or creating complex bio-sensors but requires the ability to perform droplet registration for DOD application. Section 4 demonstrated the capability to align the nozzle tip within 2 μm accuracy after successive switching of two unit print systems. To validate this capability, the right image of figure 16 shows the printed results of two buffer

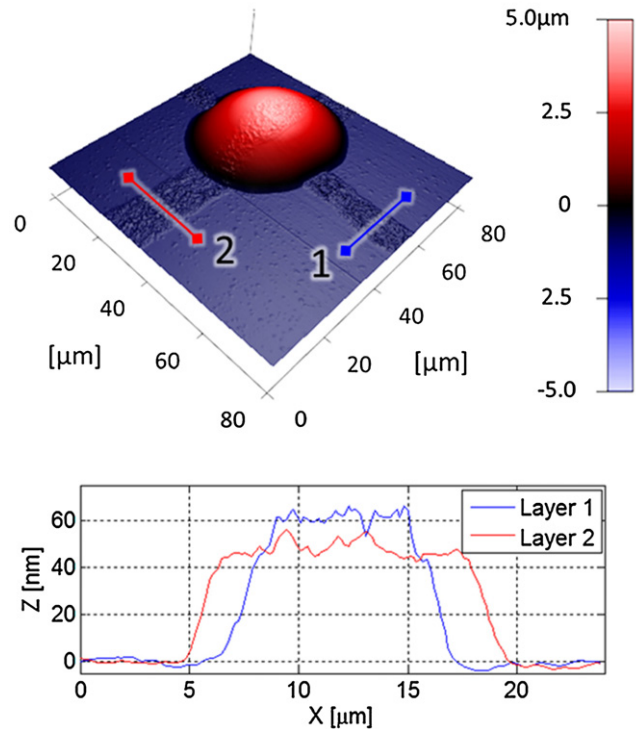


Figure 15. AFM image of the crossover structure.

solutions tagged with different fluorescent agents aligned to a grid. The solution in each unit print system A and B are Rhodamine 6G (Sigma-Aldrich) and Fluorescein Sodium Salt (Riedel-de Haén), respectively. These inks are printed on top of a silicon wafer substrate which is fluorinated with tridecafluoro-1,1,2,2-tetrahydrooctyl-1-trichlorosilane to enhance the image contrast.

The printed patterns are imaged using a fluorescent microscope (Axiovert 200M, Carl Zeiss, Inc). The microscope uses two different colour filters to differentiate the two inks. Figure 16 is produced by mixing the two colour channels (A) and (B); ink A is shown in orange and ink B is indicated by the green colour. The printed droplet diameter is approximately 2 μm, and the zoomed-in inset image validates that the registration accuracy of the droplet is well within 2 μm. The yellow colour droplets on the bottom right corner shows the two inks overlaid on top of each other in precisely the DOD approach advocated in section 1. Since the droplets can be made even smaller than the 2 μm sizes in figure 16, this registration and overlay accuracy enables researchers to automatically produce numerous micro-reactions at a very fine resolution with ease.

The final results utilize a complex test pattern to fully utilize the four-unit system designed and shown in figure 6.

Table 2. Fluorescent ink composition.

Ink	Chemical	Composition
1	Ovalbumin-Alexa Fluor 647 (Invitrogen)	5 μ M
	Glycerol	40% by volume
	Buffer solution	
	NaCl	50 mM
2	Potassium phosphate (pH = 6.9)	25 mM
	Rhodamine B (Sigma-Aldrich)	30 μ M
	Glycerol	40% by volume
	Buffer solution	
3	NaCl	50 mM
	Potassium Phosphate (pH = 6.9)	25 mM
	4',6-diamidino-2-phenylindole dihydrochloride/DAPI (Sigma-Aldrich)	75 μ M
	Glycerol	10% by volume
4	Buffer solution	
	NaCl	50 mM
	Tris-acetate (pH = 8.0)	25 mM
	Fluorescein sodium salt (Riedel-de Haën)	30 μ M
	Glycerol	40% by volume
	Buffer solution	
	NaCl	50 mM
	Potassium phosphate (pH = 6.9)	25 mM

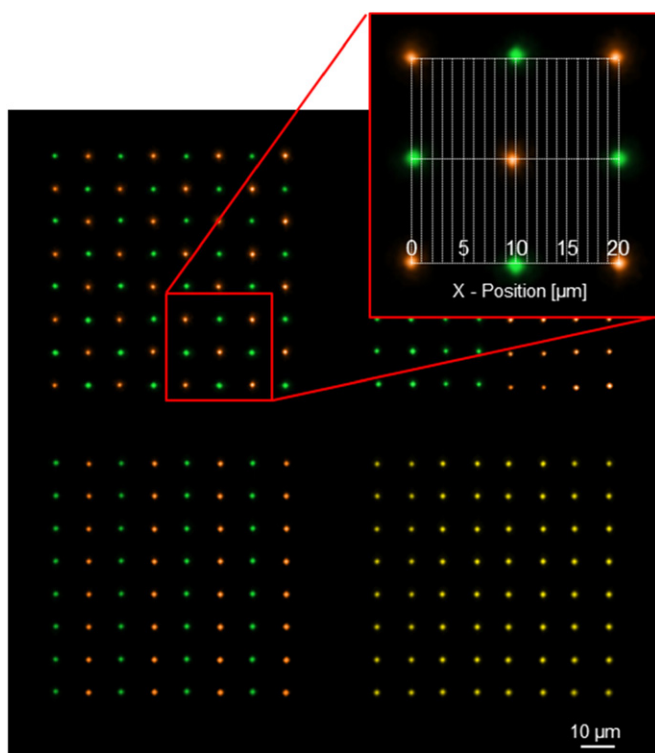


Figure 16. Microarray printing of two fluorescent agent solution.

The image shown in figure 17 is of a parrot utilizing all four print units of the system with four separately fluorescent agent inks. Details of the ink composition are listed in table 2. The image is relatively large and therefore takes some time to prepare, including the indexing among various print units. Following established E-jet processes, glycerol is added to all solutions to prevent evaporation during printing which reduces the likelihood of nozzle clogging [7]. The printed pattern is observed using a microscope with four different colour filters,

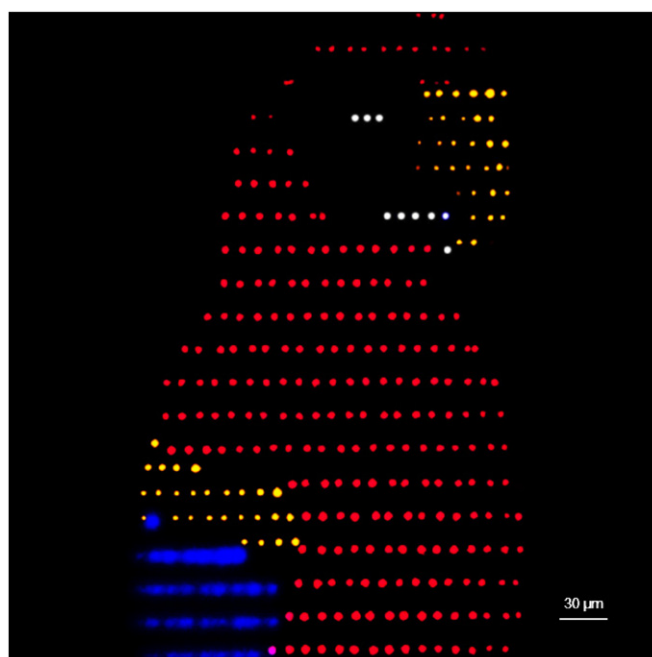


Figure 17. Complex multimaterial printing of fluorescently tagged buffer solution.

namely (1) ‘Cy5’, (2) ‘Rhodamine’, (3) ‘FITC’ and (4) ‘DAPI’. The fluorescent colour is indicated by red, orange, white and blue respectively in figure 17. As illustrated by figure 17, this multimaterial E-jet system is able to print multiple materials with the accuracy and resolution unavailable in other currently available printing techniques.

One important item related to the application of multimaterial E-jet printing is the appropriate decomposition of target patterns into individual unit printing tasks. This is a highly relevant aspect of the manufacturing technology that has been incorporated into the overall machine function. To

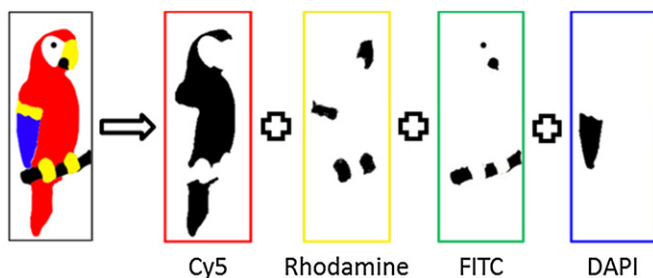


Figure 18. Image decomposition for multimaterial printing.

generate the machine code for printing the parrot pattern, for example, a bitmap image is automatically decomposed and saved to four different bitmap files as illustrated in figure 18. Using an image-to-g-code converter, the four images are converted into four g-code files that will be executed by the corresponding print unit. The top left corner of the image serves as a (0,0) origin for the printing. Details of this tool and other software supporting multimaterial E-jet can be found in [11]. Figure 17 only shows the top half of the original image due to limited field of view of the camera. The overall number of droplets for this complex figure was approximately 400 with a printing time, including switching materials of about 5 min.

6. Conclusion and future work

This work has illustrated the concept, and demonstrated the application, of multimaterial E-jet systems using multiunit print-heads. The key enablers were the mechanical design of the print-head and the operational management of the indexing system. The indexing system used a combination of micro- and macro-positioning feedback mechanisms to enable very precise indexing from one print unit nozzle to a subsequent one. With the effectiveness of the tool demonstrated, future work for this tool will explore the manufacturing space enabled by the printing technology. Additional improvements to the tool itself will include modularity and ‘quick change’ features to the print-head design as well as the automated ‘on-tool’ integration of functionalities such as in situ UV curing and interconnect sintering [23].

Acknowledgment

The author would like to acknowledge Ying He and Dr Yi Lu for supplying the fluorescent materials. Keith Parish, Kyle Cheek, Clifford Gulyash and Gary Sedberry of the MechSE machine shop for their insightful inputs on the toolbit design. Additionally, the author would also like to acknowledge the contribution and support of the NSF Nano-CEMMS Centre under award numbers SF CMI 07-49028.

References

- [1] Calvert P 2001 Inkjet printing for materials and devices *Chem. Mater.* **13** 3299–305
- [2] Creagh L T and McDonald M 2003 Design and performance of inkjet print heads for non-graphic-arts applications *MRS Bull.* **28** 807–11
- [3] Siringhaus H 2000 High-resolution inkjet printing of all-polymer transistor circuits *Science* **290** 2123–6
- [4] Mishra S, Barton K L, Alleyne A G, Ferreira P M and Rogers J A 2010 High-speed and drop-on-demand printing with a pulsed electrohydrodynamic jet *J. Micromech. Microeng.* **20** 1–8
- [5] Barton K, Mishra S, Alleyne A, Placid F and Rogers J 2010 Control of high-resolution electrohydrodynamic jet printing *Control Eng. Pract.* **1266–73**
- [6] Barton K *et al* 2010 A desktop electrohydrodynamic jet printing system *Mechatronics* **20** 611–6
- [7] Park J U *et al* 2007 High-resolution electrohydrodynamic jet printing *Nature Mater* **6** 782–9
- [8] Packard H 2010 *HP Computer Museum* <http://www.hpmuseum.net>
- [9] Graf P, Sutanto E, Barton K, Alleyne A and Ferreira P 2011 High-resolution electrohydrodynamic jet printing system *North American Manufacturing Research Con. (Corvallis)*
- [10] Choi H K, Park J U, Park O O, Ferreira P M and Georgiadis J G 2008 Scaling laws for jet pulsations associated with high-resolution electrohydrodynamic printing *Appl. Phys. Lett.* **92** 123109
- [11] Sutanto E 2011 A Multimaterial E-jet deposition system: fabrication, integration and application *Masters Thesis* University of Illinois Urbana Champaign, Urbana http://www.ideals.illinois.edu/bitstream/handle/2142/29756/Sutanto_Erick.pdf?
- [12] Ogata K 2010 *Modern Control Engineering Modern Control Engineering* (Upper Saddle River, United States of America: Prentice Hall) pp 63–99
- [13] Ogata K 2010 *Modern Control Engineering Modern Control Engineering* (Upper Saddle River, United States of America: Prentice Hall) p 419
- [14] Canny J 1986 A Computational approach to edge detection *Pattern Anal. Mach. Intell.* **6** 679–98
- [15] Kanopoulos N, Nagesh V and Baker R L 1998 Design of an image edge detection filter using the sobel operator *IEEE J. Solid State Circuits* **23** 358–67
- [16] Liberzon D and Morse A S 1999 Basic problems in stability and design of switched systems *IEEE Control Syst.* **19** 59–70
- [17] Graebe S F and Ahlen A L B 1996 ‘Dynamic transfer among alternative controllers and its relation to antiwindup controller design’ *IEEE Trans. Control Syst. Technol.* **1** 92–9
- [18] Phillips C L and Nagle H T 1995 *Digital Control System Analysis and Design* 3rd ed (Eaglewood Cliffs, United States of America: Prentice Hall)
- [19] Sutanto E, Shigeta K, Hoelzle D J, Alleyne A G and Rogers J A 2011 Micropositioning of a multimaterial electrohydrodynamic jet deposition system using vision feedback *Dynamic System and Control Conf. Arlington*
- [20] Wang K, Paine M D and Stark J P W 2009 Fully voltage-controlled electrohydrodynamic jet printing of conductive silver tracks with a sub-100 μm linewidth *J. Appl. Phys.* **106** 024907
- [21] Fuller S B, Wilhelm E J and Jacobson J M 2002 Ink-jet printed nanoparticle microelectromechanical systems *J. Microelectromech. Syst.* **11** 54–60
- [22] Park J U, Lee J H, Paik U, Lu Y and Rogers J A 2008 Nanoscale patterns of oligonucleotides formed by electrohydrodynamic jet printing with applications in biosensing and nanomaterials assembly *Nanoletters* **8** 4210–6
- [23] Allen M *et al* 2011 Contactless electrical sintering of silver nanoparticles on flexible substrates *IEEE Trans. Microw. Theory Tech* **59** 1419